RESEARCH ARTICLE

INTERNATIONAL RESEARCH JOURNAL OF MULTIDISCIPLINARY TECHNOVATION

Asian Research Association

DOI: 10.54392/rjmt26514

A Site-Friendly Approach to Assessing Mix Consistency of One-Part Geopolymer Concrete for Extrusion-Based 3D Printing

Prasad Barve [a], Deep Upadhyaya [a, *], Santosh Shah [b]

[a] Gujarat Technological University, Ahmedabad 382424, Gujarat, India
[b] OM Group, Illinois 60527, United States of America
* Corresponding Author Email: deep.upadhyaya@gtu.edu.in

DOI: https://doi.org/10.54392/irjmt26514

Check for updates

Received: 23-02-2026; Revised: 15-08-2026; Accepted: 04-09-2026; Published: 24-09-2026

Abstract: This work examines the development of an environmentally friendly one-part geopolymer concrete suitable for extrusion-based 3D printing. A total of 27 mixtures were analyzed by systematically varying precursor blends (ground granulated blast-furnace slag (GGBS) and fly ash), aggregate-to-binder ratios, and powdered activator contents. A qualitative "bucket test" was evaluated as a potentially site-friendly consistency-screening technique and showed good agreement with flow-table observations. Within the investigated material and printing conditions, a candidate printability window was associated with zero slump and a slump-flow diameter of 140–180 mm. To balance pumpability with structural build-up, the reduction in slump flow after a 10 min rest period was typically 10–15 mm for the Type-II candidate mixtures. Among the six Type-II candidates, CM-12 (50% GGBS, aggregate-to-binder ratio 1.5, and 10% activator) showed the best overall extrusion and shape-retention response and was used to print a continuous 12-layer object. Printing reduced density by 3.48–8.01% relative to mold casting, while the printed specimens showed a direction-dependent compressive response; no claim of statistically significant anisotropy is made from the available replicate set. The mold-cast mixtures developed 28-day compressive strengths of 32.7–41.29 MPa. The findings support the bucket test as a rapid preliminary screening method rather than a stand-alone predictor of successful printing. Further validation across materials, environmental conditions, and printer configurations is required before the numerical limits can be used as general site-control criteria.

Keywords: Geopolymer Concrete, 3D Printing, Printability, Mix Consistency, Flow Assessment, Compressive Strength.

1. Introduction

Geopolymer concrete is a sustainable alternative to ordinary Portland cement (OPC) products [1]. It is based on alkali-activated aluminosilicate precursor materials that form a hardened inorganic polymer network [2]. The essential chemistry involves alkaline dissolution of silica- and alumina-bearing components from industrial by-products such as fly ash, ground granulated blast-furnace slag (GGBS), and metakaolin [3]. The dissolved Si-O-Al species undergo polycondensation to form an amorphous to semi-crystalline three-dimensional aluminosilicate network [2]. This alkali-activation mechanism governs the setting and strength development of geopolymer binders. Geopolymer concrete offers considerable environmental benefits because it avoids energy-intensive clinker production and can incorporate industrial wastes as precursor materials, thereby reducing CO_2 emissions and embodied energy relative to OPC-based systems [4]. Life-cycle assessment studies have shown that optimized geopolymer formulations can reduce CO_2 emissions by up to 61% compared with comparable OPC mixtures [5]. Geopolymer concrete has also been used in precast elements, repair materials, masonry units, and emerging construction techniques such as additive manufacturing [6]. Current research focuses on precursor blends incorporating fly ash and GGBS to balance early strength development and rheology, ambient-temperature curing formulations for field applications, and mixture optimization informed by life-cycle assessment to improve sustainability [7].

Concrete 3D printing, referred to as extrusion-based additive construction technology, is a disruptive method in the building sector by which layer-by-layer cementitious materials are extruded following digitally controlled toolpaths to create structural elements with unprecedented geometric freedom [8, 9]. The technology represents the construction manifestation of Industry 4.0, where digital design, automated fabrication, sensors and process control are joined together on a single fabrication platform [10]. The benefits of 3DCP versus other construction techniques are numerous, such as there being no need for formwork, reduced construction periods, less strenuous work activities and waste material amounts, and the ease with which complex geometries and functionally graded constructions can be made compared to traditional casting methods [11]. Printable concrete must meet various fresh-state requirements, which include pumpability to allow continuous flow through delivery systems; extrudability so that the mortar is capable of being smoothly deposited without clogging or segregation; buildability, a property ensuring adequate shape retention and strength in the fabricating stage; and sufficient open time to remain workable for an extended period of time during printing [12]. These printability requirements are controlled by yield stress (important for buildability and shape retention), plastic viscosity (affects extrudability and surface finish) and thixotropy (for fast shape recovery after extrusion but prolonged workability during pumping) [13]. However, practical challenges remain in terms of achieving standardization for printability assessment methods; controlling anisotropy and interlayer bond strength; ensuring consistent material feed under changing environmental conditions; and preventing early-age curing issues on site.

One-part geopolymer concrete, also known as "just-add-water" geopolymer, makes a significant step towards making the use of alkali-activated materials practical on-site without having to manually mix and work with corrosive alkaline solutions [14]. While all conventional two-part geopolymer systems are based on the mixing of solid aluminosilicate precursors with liquid alkaline activators (commonly sodium or potassium hydroxide and silicate solutions) just prior to placement, one-part systems contain solid activators in the dry binder mix itself and only need water addition to induce dissolution and geopolymerization [15]. This fundamental difference confers multiple advantages for commercial deployment: enhanced safety by avoiding handling of highly caustic liquids, improved storage stability of the dry binder, simplified mixing procedures analogous to OPC-based systems, and greater site-friendliness, particularly for remote or resource-constrained construction environments [16]. It has been found that solid activators recently employed in such compositions include different grades of powdered sodium silicate and anhydrous sodium metasilicate, which, upon hydration, will produce the soluble alkali and silicate species necessary to activate the aluminosilicate precursors [16]. However, the design of the one-part geopolymer systems faces specific challenges compared to two-part systems, such as obtaining good dissolution kinetics for solid activators at room temperature, controlling setting time in order to balance workability and early-age strength development, and optimizing fresh-state rheology to coincide with the placement methods. Recent research has focused on ambient-cured one-part formulations specifically tailored for extrusion-based applications, strategic blending of fly ash with GGBS to accelerate early strength development while maintaining workability, and the exploration of alternative industrial waste streams as supplementary precursors [17, 18].

Combining one-part geopolymer binders with extrusion-based 3D printing offers a means of integrating sustainability objectives with advanced manufacturing capabilities and can facilitate on-site construction using low-carbon materials [19]. For this integration to be successful, however, the rheological response and mixture-design variables must be carefully optimized to satisfy competing printability requirements. A printable one-part geopolymer should have sufficiently low initial viscosity and yield stress for pumping, followed by sufficient yield stress and structural recovery after extrusion to retain its shape and support successive layers, while maintaining an adequate open time for continuous printing without premature stiffening [20]. Fresh-state characteristics and subsequent mechanical performance are strongly influenced by the selection and proportioning of constituents. GGBS supplies calcium and can accelerate reaction and early strength development, thereby improving buildability and load-bearing capacity, whereas fly ash generally improves workability and pumpability and contributes to slower strength development. Accordingly, the fly ash-to-GGBS ratio must be optimized carefully. Higher activator dosages can accelerate geopolymerization but may also shorten setting time and increase sensitivity to curing conditions [21]. The aggregate-to-binder ratio affects extrudability, interlayer bonding, surface finish, and strength and must therefore be optimized with respect to nozzle size, layer thickness, and deposition speed [22]. Anisotropic behavior has been reported in 3D-printed geopolymer elements under compression, flexure, and tension, with mechanical properties varying according to the orientation of loading relative to the printing direction because of weaker bonding between successive layers [23]. Recent studies have shown that engineered one-part geopolymers can achieve structural-grade compressive strength while offering potential environmental benefits, including reductions of up to 61% in CO_2 emissions and approximately 14% in embodied energy compared with equivalent 3D-printable OPC-based systems [7].

Although substantial progress has been made in the development of 3D-printable geopolymer concrete, there remains a need for rapid, low-cost, on-site techniques to evaluate mixture workability and printability. Traditional workability tests, such as slump and flow-table measurements, are useful for preliminary material screening but cannot fully characterize the rheological behavior that governs shape retention, structural recovery, and buildability during layer-by-layer printing. Rheometric characterization of yield stress, plastic viscosity, and thixotropy is highly informative, but it requires specialized equipment, trained personnel, and relatively large material batches, which limits its practicality for routine quality control on construction sites [24-26]. Direct extrusion and printing experiments provide the most representative assessment of printability but are time- and material-intensive and require dedicated printing equipment, limiting their use for rapid mixture optimization and real-time process control. In addition, one-part geopolymer systems are sensitive to placement conditions, solid-activator reaction kinetics, and precursor composition, which can affect fresh-state behavior during field operations. There is therefore a practical need for simple indirect tests that use small quantities of material and basic equipment and can be performed by non-specialized personnel. Such approaches could support rapid mixture screening during formulation development, identify unsuitable batches during production, and facilitate real-time decisions during printing operations, thereby supporting the wider deployment of 3D-printed geopolymer construction. The present work is intended to contribute toward the development of practical procedures for assessing 3D-printable mixtures.

The current work addresses this gap by proposing and evaluating a simplified, site-friendly bucket-test protocol for indirect assessment of mix consistency related to pumpability and extrudability using limited quantities of material. A systematic experimental study was performed using 27 one-part geopolymer concrete mixtures with controlled variations in activator level, aggregate-to-binder ratio, and precursor proportion. Bucket-test classifications were compared with slump and slump-flow measurements, and the six Type-II candidate mixtures were subsequently examined by single-filament printing using a large-scale gantry 3D concrete printer. The printing trials showed that Type-II classification was useful for identifying candidate mixtures, but it did not by itself guarantee continuous extrusion and acceptable filament stability. Accordingly, the proposed method is treated as a rapid preliminary consistency-screening tool that should be used together with quantitative flow measurements and printing verification, rather than as a substitute for rheometric characterization.

2. Materials and methodology

2.1. Mixture proportions and sample preparation

The one-part geopolymer binder was synthesized using the commercially available Pozzocrete® 60 fly ash, which is produced in India by Dirk India and complies with IS 3812 (Part-1):2013, and GGBS, which complies with IS 16715:2018. These materials are obtained from local suppliers in Gujarat state, India, and were used in different quantities as silicoaluminate precursors. The geopolymer was prepared using silica sand as a fine aggregate. For this investigation, powdered sodium metasilicate (Na2SiO3) anhydrous (Na2O:SiO2 = 1:0.9371, according to the supplier) from Associated Finechem Pvt. Ltd., Gujarat, India, served as the only one-part activator. Sucrose powder was used as a retarder to increase the open time of the one-part geopolymers [20, 27].

Table 1. Oxide (%) compositions of the raw materials determined by XRF

	SiO_2	CaO	Al_2O_3	Fe_2O_3	K_2O	MgO	Na_2O	SO_3	TiO_2	P_2O_5	MnO
FA	60.67	1.50	28.76	4.84	0.53	0.90	0.56	0.39	1.07	0.38	0.13
GGBS	39.38	23.11	19.64	0.62	0.47	11.00	1.54	3.45	0.37	0.01	0.01

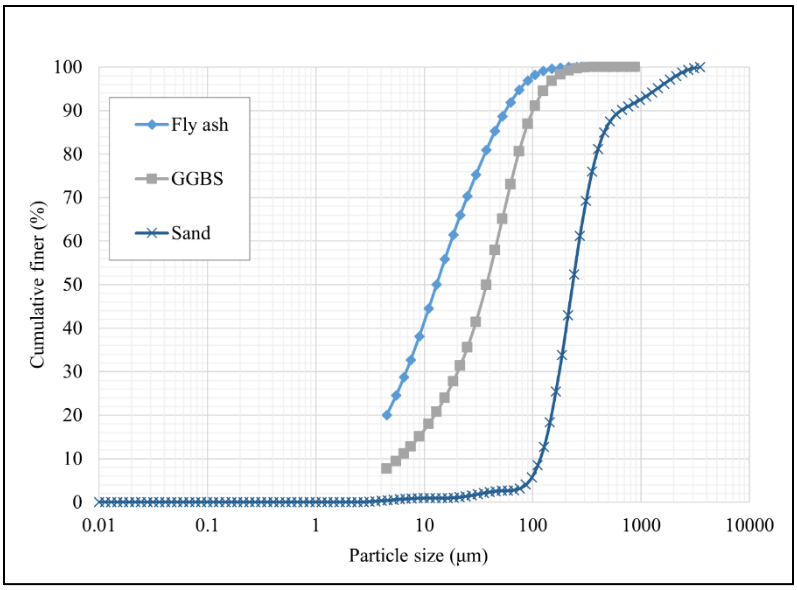

Figure 1. Particle size distributions of fly ash, GGBS and sand

Table 1 shows the chemical composition of fly ash and GGBS as determined by the PANalytical Axios Max Wavelength Dispersive X-Ray Fluorescence (XRF) Spectrometer with Standardless Omnian analysis software. GGBS and fly ash had specific gravities of 2.86 and 2.3, respectively. Figure. 1 displays the particle size grading curves for GGBS and fly ash as determined by a laser diffraction particle size analyzer (Sympatec-HELOS (H1004) & Sucell-BF, Germany) with a particle size range of 0.1 µm to 875 µm, while Malvern Panalytical Mastersizer - v3.88 was used for fine sand. Fly ash and GGBS were found to have median diameters (D50) of 12.98 µm and 37.56 µm, respectively.

Following prior examination, 27 formulations of one-part geopolymer concrete with varying activator levels (10%, 15% and 20% weight of binder) and aggregate: binder ratios = 1.25, 1.50 and 1.75, as shown in Table 2, were employed in this study to pre-determine the printable zone. As a partial substitute for fly ash, the GGBS was added at proportions of 10%, 30%, and 50% of the precursor, respectively. Here, all the mixes had the same amount of precursor. The requisite dosage of retarder was derived from earlier investigations [7, 20, 28] and using a trial-and-error process. In the present formulation study, the water content was fixed at 140 g for all 27 mixtures to provide a common liquid-water basis during the preliminary identification of the printable mixture zone. This approach was adopted deliberately to avoid introducing water dosage as an additional variable while systematically varying the sodium metasilicate dosage, GGBS content, and aggregate-to-binder ratio. Because the activator was used as anhydrous Na2SiO3 powder, increasing its dosage from 10% to 20% at constant water content necessarily reduced the water-to-activator ratio and increased the concentration of dissolved alkaline silicate species in the liquid phase. Consequently, the nominal activator percentage should not be interpreted independently of the available water. The resulting changes in ionic concentration, particle dispersion, free-water availability, and early reaction kinetics can simultaneously influence flowability, yield stress, structural build-up, setting, and extrusion behavior [29-31]. Recent studies have demonstrated that the rheology of alkali-activated slag systems is strongly governed by activator concentration, silicate chemistry, and the distribution of free water, with changes in these parameters affecting particle interactions and early-age structural development [29, 30]. Similar effects are particularly relevant to extrusion-based 3D printing, where the balance between flowability during pumping/extrusion and rapid structural build-up after deposition determines extrudability and buildability [31]. Therefore, the observed differences among the 27 mixtures represent the combined effect of nominal Na2SiO3 dosage, its corresponding dissolved concentration at a fixed water content, precursor composition, and aggregate packing, rather than the isolated effect of activator percentage. The constant-water strategy was thus used as a controlled screening approach to identify a practical printable zone, while the resulting coupled effects of water availability and activator concentration were considered when interpreting the fresh-state and printing performance. Using a Hobart mixer, the mixing process was carried out in the following three steps: First, all of the ingredients, aside from GGBS, were blended dry for two minutes at a low speed. After that, add 85% of the entire water and mix at medium speed for a further ten minutes. Finally, GGBS was added, and in order to create a uniform mixture, the remaining water was added gradually while the high-speed mixing proceeded. As reported in previous studies [20], the residual water keeps the mixture from becoming unworkable due to the dissolving of the powder activator. This is mainly to ensure that during the mixing process, the powder activator dissolves thoroughly [20]. Because GGBS is more reactive than fly ash, it might take in the majority of the silicate, leaving fly ash with insufficient material to react with and produce an inferior geopolymer product [32]. For this reason, GGBS is not added at the beginning.

2.2. Mix consistency for printability

Pumpability is the ability of a fresh printing mixture to be transported through the delivery system under pressure without blockage, segregation, or unacceptable changes in its properties [11]. For concrete 3D printing, the material must be sufficiently flowable for transport by pumping while remaining stiff enough after extrusion to retain the deposited filament shape. Extrudability refers to the ability of the material to pass continuously through the printhead and form an uninterrupted filament without blockage or segregation [11]. Pumpability and extrudability are therefore essential requirements for successful printing. In large-scale systems, such as gantry-based or robotic-arm printers, continuous mixing and pumping are typically required. This differs from many small-scale laboratory printers, in which material is prepared separately and manually fed into a hopper. Therefore, the mixture-consistency requirements of these two systems can differ substantially. Moreover, evaluating every mixture directly on a large-scale printer is difficult and uneconomical because each trial requires a relatively large quantity of material. Empirical guidelines for achieving suitable printability have consequently been proposed in the literature [33].

In this study, the bucket test was developed as an indirect, site-oriented method for assessing mix consistency related to pumpability and extrudability. Approximately 1.0–1.25 L of freshly mixed material was placed in a galvanized-iron or mild-steel bucket with a top diameter of 350 mm and a depth of 100 mm (nominal capacity 15–20 L), as shown in Figure. 2(a).

Table 2. Mixture combinations of one-part geopolymer concrete

Mixture ID	Fly ash (gm)	GGBS (gm)	Sand (gm)	Water (gm)	Activator (gm)	Sucrose powder (% of precursor)
CM-1	360	40	500	140	40	1.0
CM-2	280	120	500	140	40	1.0
CM-3	200	200	500	140	40	1.0
CM-4	360	40	500	140	60	1.0
CM-5	280	120	500	140	60	1.0
CM-6	200	200	500	140	60	1.0
CM-7	360	40	500	140	80	1.0
CM-8	280	120	500	140	80	1.0
CM-9	200	200	500	140	80	1.0
CM-10	360	40	600	140	40	1.0
CM-11	280	120	600	140	40	1.0
CM-12	200	200	600	140	40	1.0
CM-13	360	40	600	140	60	1.0
CM-14	280	120	600	140	60	1.0
CM-15	200	200	600	140	60	1.0
CM-16	360	40	600	140	80	1.0
CM-17	280	120	600	140	80	1.0
CM-18	200	200	600	140	80	1.0
CM-19	360	40	700	140	40	1.0
CM-20	280	120	700	140	40	1.0
CM-21	200	200	700	140	40	1.0
CM-22	360	40	700	140	60	1.0
CM-23	280	120	700	140	60	1.0
CM-24	200	200	700	140	60	1.0
CM-25	360	40	700	140	80	1.0
CM-26	280	120	700	140	80	1.0
CM-27	200	200	700	140	80	1.0

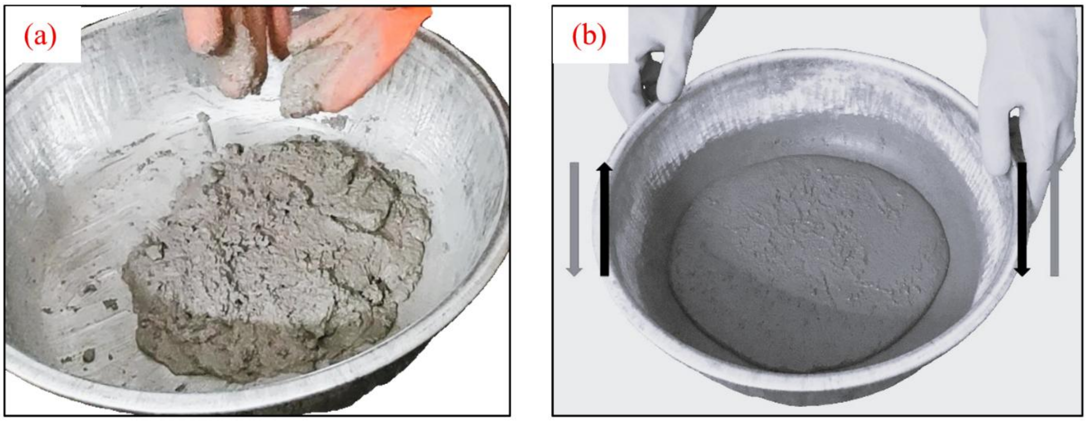

Figure 2. Bucket test for the mix consistency related to printability.

Immediately after mixing, the bucket base was kept in full contact with the floor and the bucket was rocked in a seesaw motion at approximately 1–2 shakes per second until the mixture first became level, as shown in Figure. 2(b). No pause was introduced between mixing and the shaking step. Because the time required to reach a level surface varied with mixture consistency, shaking duration was not fixed; instead, the leveling endpoint was used and the time-to-level was treated as part of the qualitative response. After leveling, the observations described in Section 3.1 were performed in a fixed sequence. The test should therefore be interpreted as a standardized qualitative screening procedure with an endpoint-based shaking step, rather than as a quantitative rheological measurement.

2.3. Flow assessment

The two main competing requirements for 3D-printable concrete mixtures are pumpability and buildability, both of which depend on fresh-state properties [34]. Slump measurements can provide an indication of buildability and static yield stress, whereas slump-flow measurements can be related to pumpability and dynamic yield stress [35]. Accordingly, a flow-table apparatus conforming to IS 5512:1983, shown in Figure. 3(a), was used to determine the flow characteristics of all 27 fresh mixtures in accordance with IS 4031 (Part 7):1988. The test procedure was as follows. Fresh mortar was placed in two layers in a mini-slump cone measuring 50 mm in height, with top and bottom diameters of 70 and 100 mm, respectively (Fig. 3(b)). Each layer was tamped using a rod 12.5 mm in diameter and 125-150 mm long with a rounded working end. After filling and compacting both layers, excess mortar was removed with a straightedge so that the surface was flush with the top of the cone (Figure. 3(c)). Slump was defined as the difference between the mold height and the height of the mortar after removal of the cone. The flow table was then dropped 25 times, and slump flow was recorded as the average diameter of the mortar measured along the scribed lines on the tabletop (Figure. 3(d)). The mold was lifted 1 min after completion of mixing, after which the table was immediately dropped 25 times within 15 s. This controlled timing was maintained for all tests to minimize the influence of time-dependent rheological changes. Based on the bucket-test observations and slump-flow measurements, a candidate printability zone was proposed.

2.4. Visual Examination for Printability Evaluation and Printing-Based Assessment of the Candidate Printable Zone

The six Type-II mixtures identified by the bucket test and flow assessment were subjected to printing-based evaluation of the candidate printable zone. Single filaments with a target geometry of 1000 mm (L) × 30 mm (W) × 20 mm (H) were printed and examined for material delivery, extrusion continuity, filament spreading, surface condition, and shape retention. The mixture with the best overall printing response was then assessed for buildability by printing a hollow rectangular object measuring 800 mm (L) × 200 mm (W). A three-axis gantry-type large-scale extrusion-based concrete 3D printer was used, as illustrated in Figure. 4. A pan mixer produced a uniform mixture before transfer to the hopper. The motor-driven auger extruder received material from the hopper through a progressive-cavity pump and a 5 m long, 50 mm diameter hose, and the material was discharged through a 30 mm circular nozzle. The printer has a working capacity of 10 m (W) × 5 m (H) × L (variable). Printing speed was maintained at 90 mm/s, material flow rate at 3.24 L/min, and pumping pressure at 1.3 bar for all mixtures evaluated by extrusion. These printing trials were used to assess the practical performance of the screened candidates; they were not treated as a full validation dataset for estimating sensitivity or specificity of the bucket-test classification.

2.5. Compressive strength

To determine the 28-day compressive strength of the printable mixtures, 50 × 50 × 50 mm³ cubes were mold cast. The anisotropic response of the 3D-printed specimens was assessed using cylindrical cores obtained from printed slabs and tested in longitudinal, lateral, and perpendicular orientations, as illustrated in Figure. 5. Core strength was calculated in accordance with IS 516 (Part 4): 2018 from the maximum load divided by the measured cross-sectional area. For cores with diameter below 70 mm, the measured cylinder strength was multiplied by the IS 516 diameter correction factor of 1.06; the corrected cylinder strength for specimens with height/diameter = 2 was then multiplied by 5/4 to obtain an IS 516-equivalent cube strength. The tested printed cores measured 65 mm in diameter and 130 mm in height. Three specimens were tested for each orientation and the mean value was reported. Because these conversion factors originate from a conventional-concrete standard and no geopolymer-specific core-to-cube calibration was performed in the present study, the converted printed strengths should be interpreted as IS 516-equivalent values for within-study comparison rather than as a separately validated geopolymer-specific cube-strength conversion.

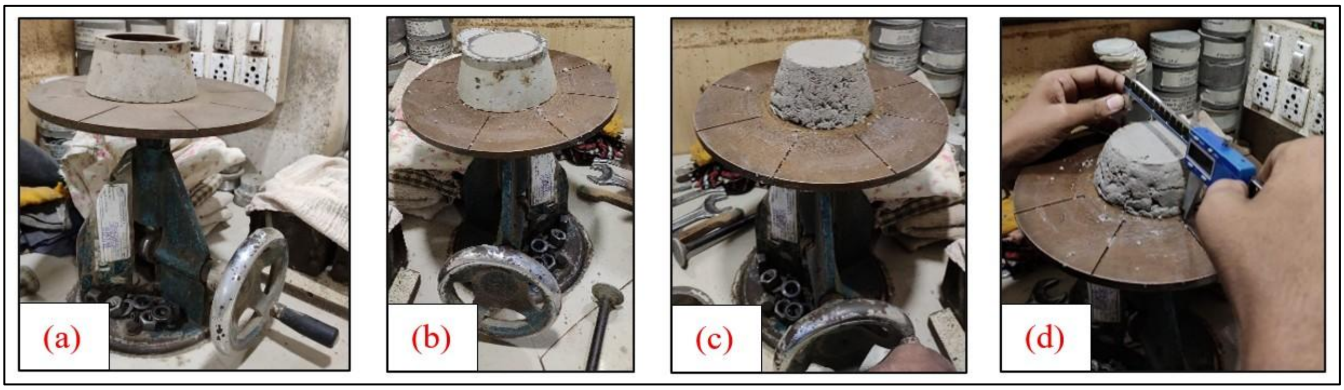

Figure 3. Set-up and performance of slump and slump flow test on one-part geopolymer concrete

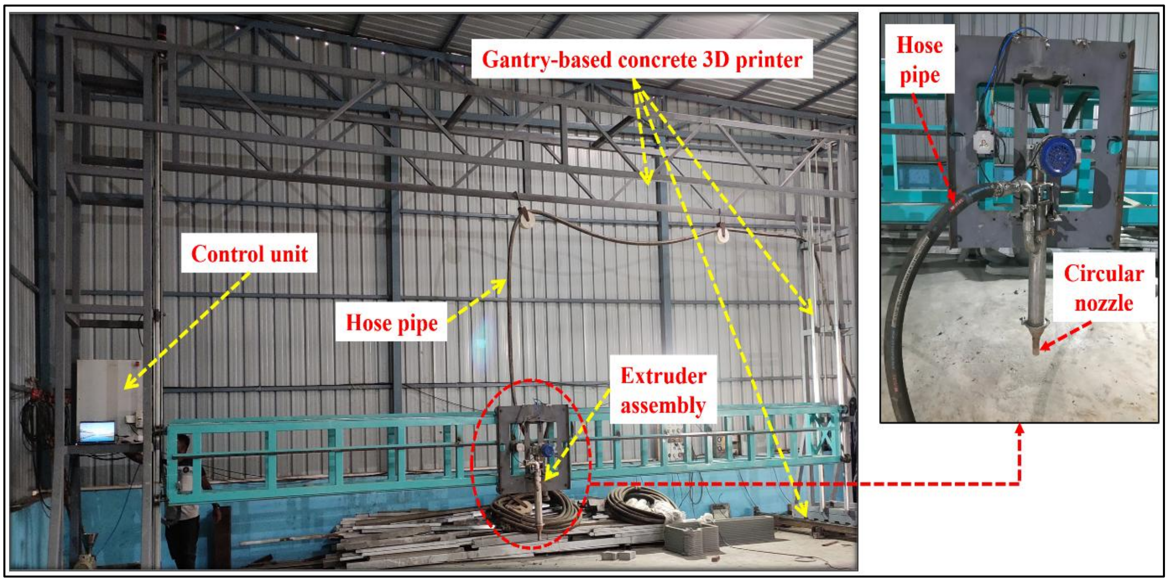

Figure 4. Gantry-based concrete 3D printer employed for current research.

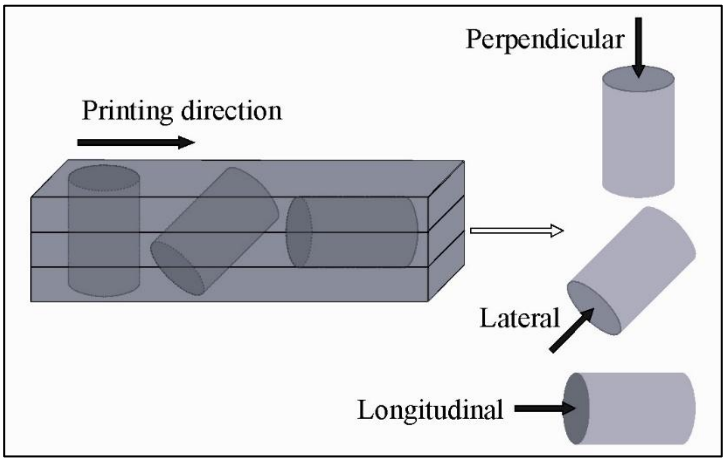

Figure 5. Diagrammatic representation of samples taken from printed slabs and their compressive strength testing orientations.

Laboratory conditions were 27 ± 2 °C and 65 ± 5% relative humidity. The compression testing machine complied with IS 14858:2000, had a maximum load capacity of 3000 kN, and was operated at 0.583 kN/s in accordance with IS 516 (Part 1/Sec 1):2021.

3. Results and Discussion

3.1. Bucket Test Findings

The bucket-test observations are shown in Figure. 6 and the mixtures were classified as Type-I, II, III, or IV. After the mixture first reached a level surface, it was observed for 60 s for visible segregation or bleeding. Any mixture showing segregation or bleeding was classified as Type-I and rejected from further printability screening. The bucket was then immediately rotated to an approximately vertical position (about 90° to the floor) and the gravity-driven movement of the mixture was observed. A Type-II candidate was defined by the whole mass sliding as a cohesive body without visible separation and without substantial material remaining adhered to the bucket surface. After returning the bucket to the horizontal position, the surface was immediately scratched once with a fingertip and gently pressed to assess whether coarse sand had segregated to the bottom and whether the furrow closed immediately. These tactile observations were used only as supporting qualitative indicators; they were not treated as quantitative measurements of viscosity, yield stress, or thixotropy. Mixtures that were sticky/highly fluid or failed the cohesive sliding criterion were assigned to Type-III, while very stiff or rapidly setting mixtures that did not slide under gravity were assigned to Type-IV.

Type-III behavior included mixtures in which part of the material adhered to the bucket while the remaining mass moved downward, indicating poor consistency for the tested delivery system, or mixtures that were excessively fluid and unable to retain filament shape. Type-IV behavior was assigned when the mixture was sufficiently stiff or rapidly setting that it did not slide under gravity.

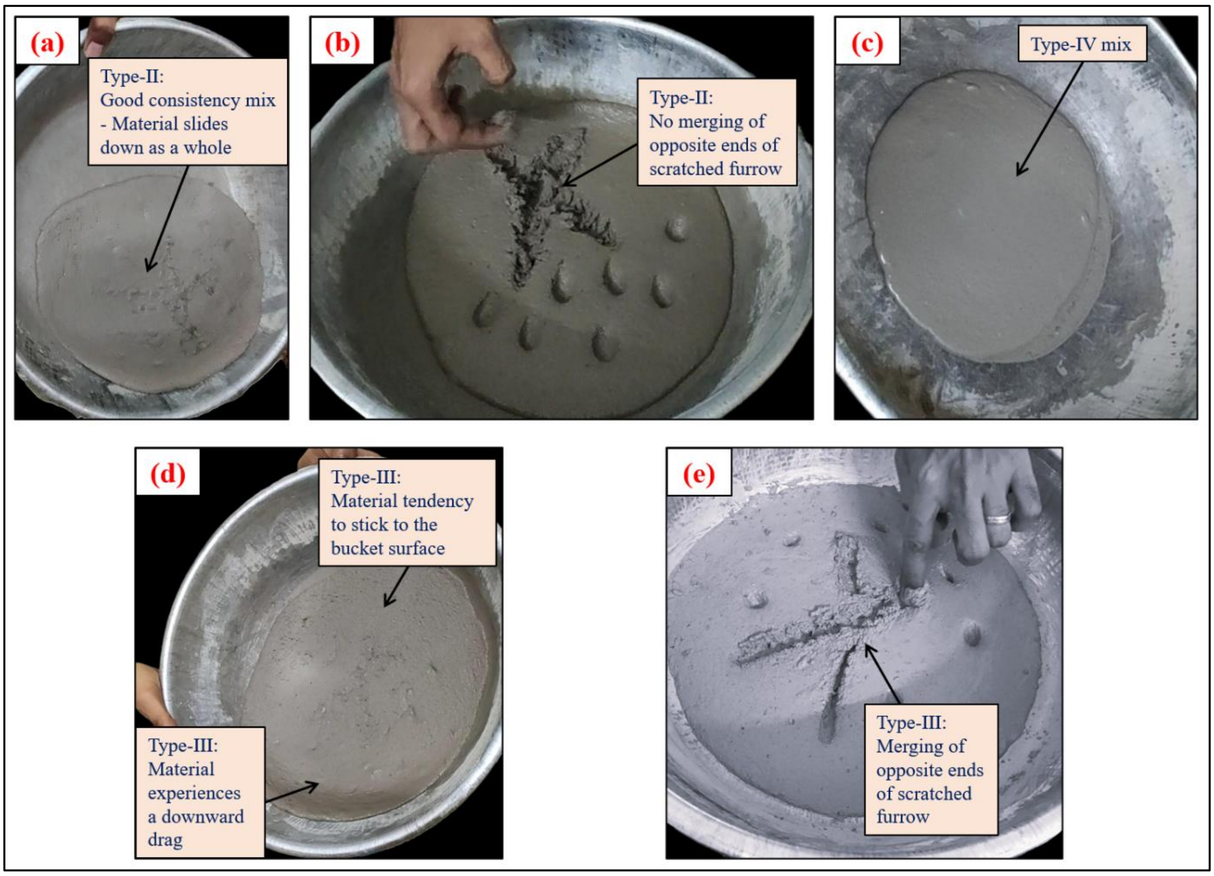

Figure 6. Bucket test findings for the mix consistency related to printability.

Because adhesion, tactile roughness, and furrow closure are still operator-observed features, the bucket test remains a qualitative screening method; the flow-table and printing trials were therefore used as complementary checks.

The 27 formulated mixtures of one-part geopolymer concrete were divided into 8 sets depending on bucket test observations. Set-1 included CM-1, CM-2 and CM-3 mixes. CM-1 and CM-2 exhibited a high spreading tendency and bleeding. Since, the aggregate: binder ratio was 1.25, the greater paste volume and lesser volume fraction of sand can result in low yield stress adversely affecting shape retention ability, even though having good pumpability and extrudability. Though, CM-3 had the same aggregate: binder ratio, it had lesser flowability compared to CM-1 and CM-2 mixes due to the higher GGBS content.

Set-2 comprised of CM-4, CM-5 and CM-6, in which the CM-4 mix had considerable flowability owing to higher fly ash content, while the activator level increased to 15% weight of binder. However, the CM-5 and CM-6 grew relatively stickier given the high activator and GGBS proportions, which shall require high pump capacity and pumping pressure.

CM-7, CM-8, and CM-9 were included in Set-3. CM-7 exhibited desirable behavior with no bleeding. Its adequate flowability for pumping and extrusion was attributed to the high fly ash fraction and the use of the retarder despite the higher activator dosage. As the activator dosage increased to 20% by weight of binder and the GGBS content also increased, CM-8 and CM-9 became highly viscous and stiff and tended to set rapidly, which could cause disruptions during pumping and extrusion.

CM-10, CM-11 and CM-12 were held in Set-4 with an aggregate: binder ratio of 1.5. Though the sand proportion increased in comparison to Set-1, set-2 and set-3, the high fly ash content in CM-10 made it flowable, with visible bleeding. Further, CM-11 also showed a similar behavior as CM-10. CM-12 demonstrated desirable behavior owing to adequate fly ash and GGBS proportions, aggregate: binder ratio and role of retarder.

Set-5 consisted of CM-13, CM-14 and CM-15. CM-13 displayed minor bleeding due to lower GGBS portion compared to fly ash. The increased quantity of activator to 15% caused CM-15 to be sticky and viscous in nature. While CM-14 showed desirable property with no bleeding but was stickier and viscous in comparison to CM-13.

Set-6 comprised CM-16, CM-17, and CM-18. All three mixtures were highly viscous and stiff and tended to set rapidly, which could lead to clogging of the hose or nozzle outlet.

CM-19, CM-20, and CM-21 were included in Set-7. Because of the high aggregate-to-binder ratio in Set-7, CM-19 and CM-20 exhibited a rough texture during fingertip assessment, indicating the presence of sand particles near the bottom of the mixture. CM-21 was also relatively coarse but exhibited desirable behavior without segregation or bleeding.

All the remaining mixes of Set-8 comprising of CM-22, CM-23, CM-24, CM-25, CM-26, and CM-27 were granular or coarser in nature due to greater aggregate portion and lower paste volume, resulting in high yield stress that may cause high friction while pumping and extrusion adversely affecting the printability. Further, as the activator content increased, the mixes grew highly viscous, stiff and tend to set rapidly which can result in blockages during pumping and extrusion. Finally, each mix is categorized as per the bucket test findings into Type-I, II, III, and IV, as discussed above and presented in Table 3.

The bucket test presents a simplified and rapid indirect approach to assess the mix consistency required for desired printability with the use of a very small quantity of material. Moreover, it does not demand the use of sophisticated and costly equipment and skilled labor. It proves to be site-friendly, time efficient and economical. The bucket test findings are supported with flow table and printability (pumpability and extrudability) measurements in the following sub-sections of the article.

3.2. Flow determination and printable zone

The slump and slump flow test was performed on the fresh mixes as per the procedure outlined in sub-section 2.3, to correlate and confirm the bucket test findings. Further, the reduction in flow value after a rest time of 10 minutes was also recorded to understand the setting behavior of the formulated mixes. The mixes CM-1, CM-2, CM-10, CM-11 and CM-13, exhibited a slump of 16 mm, 13 mm, 12 mm, 7 mm and 3 mm, respectively. All other mixtures had a flow diameter of 100 mm recorded prior to table drop without adjusting the water-to-binder ratio, which indicates zero slump since no flow was noticed when the cone was raised.

The Type-I mixtures CM-1, CM-2, and CM-10 showed comparatively high flow values of 186, 177, and 181 mm, respectively. This high flowability was consistent with the bucket-test observations, in which bleeding was noted. These mixtures contained relatively high fly ash proportions and 10% activator; CM-1 and CM-2 also had an aggregate-to-binder ratio of 1.25. The Type-I mixtures showed a flow reduction of approximately 7-12 mm after a 10 min rest period. This smaller reduction in flow may be associated with a slower geopolymerization rate and prolonged setting, which can adversely affect buildability and shape retention. Type-II formulations exhibited zero slump and slump-flow values of 155-176 mm. CM-7, CM-12, CM-14, and CM-21 had flow values of approximately 155-158 mm, whereas CM-3 and CM-4 showed flow values of 171 and 176 mm, respectively. The difference between CM-3 and CM-4 may be related to the higher GGBS content and lower activator dosage in CM-3. For the Type-II mixtures, the reduction in slump flow after a 10 min rest period was 11-14 mm. Although the Type-III mixtures also exhibited zero slump, their flow behavior differed. CM-5, CM-6, and CM-15 showed larger flow reductions of 16-20 mm after 10 min, indicating a faster loss of flowability that could contribute to pumping and extrusion difficulties. This behavior may be associated with the higher activator and GGBS contents of these mixtures. In contrast, CM-19 and CM-20 had initial flow values of 173 and 165 mm and reductions of 7 and 9 mm, respectively, after 10 min, indicating slower structural build-up that may compromise buildability. These mixtures contained more fly ash and less activator than CM-5, CM-6, and CM-15. The Type-IV mixtures exhibited zero slump and slump-flow values of 126-152 mm. All Type-IV mixtures showed reductions of 16-22 mm after a 10 min rest period. Reductions of 19, 21, and 20 mm were recorded for CM-9, CM-18, and CM-27, respectively; each of these mixtures contained 20% activator by weight of binder. Overall, the slump and slump-flow results were consistent with the bucket-test observations.

Based on past trials experience of large-scale printing, it was found that a printable mix demanded no-slump concrete and a slump flow between 140 – 180 mm. Similar observations were reported in the literature [36]. Moreover, it was also observed that the reduction in slump flow value after a rest time of 10 minutes must typically lie within the 10-15 mm range. Therefore, the combinations that did not meet the slump flow values specified above were ultimately rejected. Consequently, the satisfactory slump results in line with the bucket test findings were used to define the mix's printable zone as shown in Figure. 7.

The six Type-II mixtures were subjected to printing trials, and their actual outcomes demonstrated that the bucket classification identified candidates rather than guaranteeing successful printing, as shown in figure 8.

Table 3. Classification of formulated mixtures based on bucket test findings

Category	Mixture ID
Type-I	CM-1, CM-2, CM-10, CM-11, CM-13
Type-II	CM-3, CM-4, CM-7, CM-12, CM-14, CM-21
Type-III	CM-5, CM-6, CM-15, CM-19, CM-20
Type-IV	CM-8, CM-9, CM-16, CM-17, CM-18, CM-22, CM-23, CM-24, CM-25, CM-26, CM-27

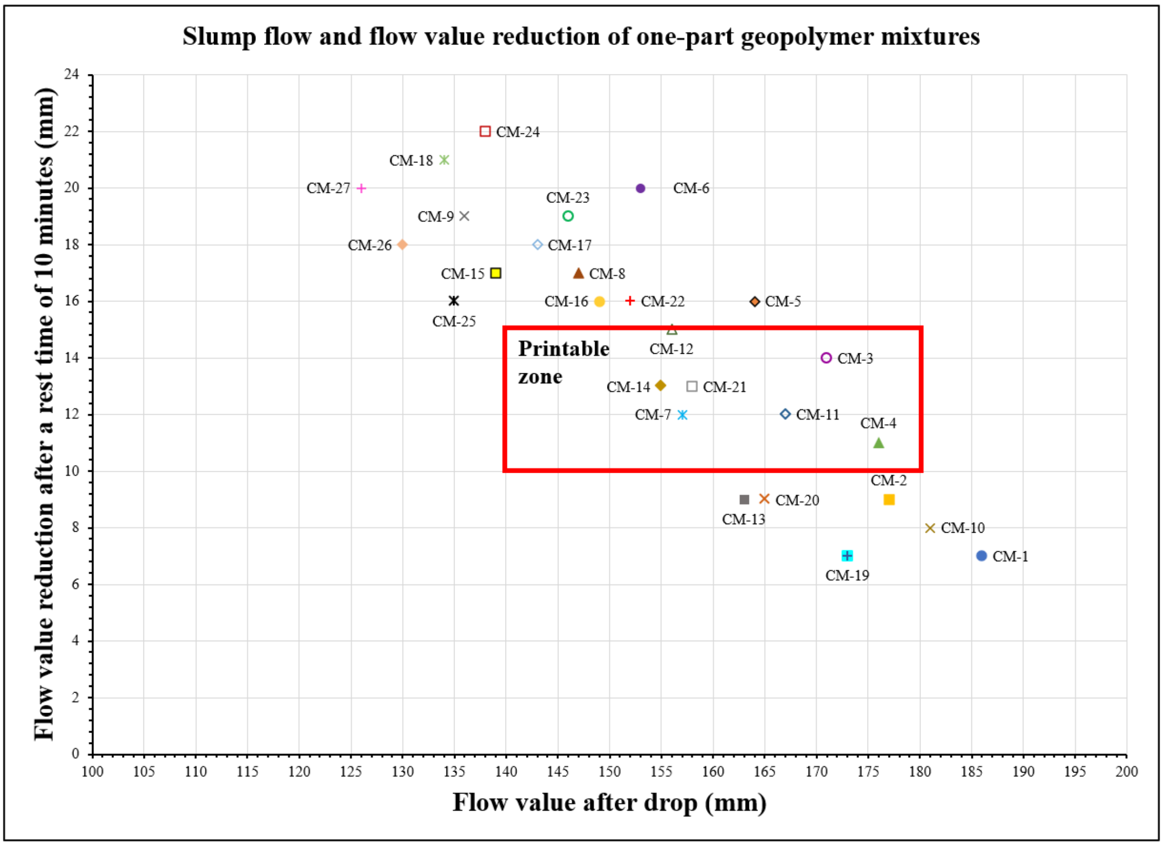

Figure 7. Printable zone of one-part geopolymer mixtures.

Figure 8. Visual examination for printability evaluation of the printable zone mixtures.

Table 4. Comparison of Type-II bucket-test classification with observed single-filament printing outcomes.

Mixture	Bucket class	Delivery to nozzle	Extrusion continuity	Observed filament outcome
CM-3	Type-II	Yes	Continuous	Average width 44 mm; spreading; poor shape retention
CM-4	Type-II	Yes	Continuous	Average width 38 mm; spreading; poor shape retention
CM-7	Type-II	Yes	Disrupted	Average width 52 mm; unstable deposition
CM-12	Type-II	Yes	Continuous	Average width 30 mm; retained shape; smooth surface
CM-14	Type-II	Yes	Discontinuous	Average width 28 mm; smooth surface but discontinuous
CM-21	Type-II	Yes	Continuous	Average width 30 mm; retained shape; harsh/dry surface

CM-3 and CM-4 were readily delivered and extruded but spread after deposition, giving average filament widths of 44 mm and 38 mm, respectively, and therefore did not provide acceptable shape retention relative to the 30 mm target width. CM-7 reached the printhead but extrusion was disrupted, with an average filament width of 52 mm. CM-12 showed continuous delivery and extrusion, an average filament width of 30 mm, good shape retention, and a smooth surface. CM-14 produced a smooth filament with an average width of 28 mm but exhibited discontinuity during printing. CM-21 was delivered and extruded continuously, retained an average width of 30 mm, and maintained its shape, although its surface was comparatively harsh and dry. Using a strict outcome criterion requiring material delivery to the nozzle, continuous extrusion, and acceptable filament stability, only CM-12 and CM-21 met all three criteria (2 of 6 Type-II candidates). Thus, Type-II classification should be interpreted as preliminary screening of potentially printable mixtures, not as a validated prediction of successful printing. Table 4 summarizes the observed outcomes. The original test campaign recorded average filament width but did not systematically record post-deposition filament height or dimensional variation along the full 1000 mm filament; no estimated values have therefore been introduced for those quantities.

The above findings indicate that CM-12 exhibited the most favorable overall printability among the mixtures evaluated. Consequently, CM-12 was further assessed for buildability by printing a hollow rectangular object measuring 800 mm (L) × 200 mm (W). Figure. 9 shows the laboratory-scale printing of the one-part geopolymer concrete object using CM-12. A 240-mm-high object comprising approximately 12 consecutive layers was printed continuously and uniformly, with no visible interruptions between layers. The deposition time was approximately 23 s per layer, and the total printing duration was 4.5 min. The nominal layer dimensions were 30 mm in width and 20 mm in height, with no noticeable layer deformation.

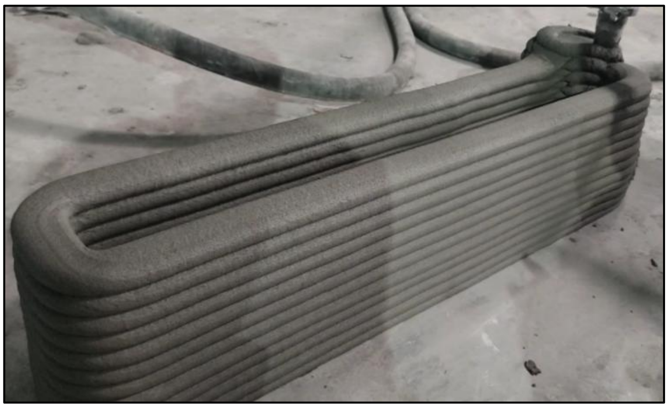

Figure 9. 3D printed object using CM-12 mix

3.3. Effect of Precursor, Aggregate to Binder Ratio and Activator Content on Printability, Setting Time, Density and Mechanical Performance

To make extrusion-based 3D printing work for geopolymer concrete, many compositional variables must be carefully coordinated to meet the strict and often conflicting needs of additive manufacturing processes. 3D printing requires materials that can be pumped for transport, extruded for filament formation, built for layer stacking and interlayer adhesion all at the same time. This is a multidimensional optimization challenge that severely limits the possible compositional space. In contrast, conventional casting allows for independent control of flowability and compaction through vibration and formwork confinement. The current study evaluated 27 mix formulations featuring systematic variations in activator content (10–20 wt.%), GGBS proportion (10–50%), and aggregate to binder ratio (1.25–1.75), of which 6 mixes attained printability. The limited success rate emphasizes the narrow processing window inherent in geopolymer binder systems and underscores the essential need to comprehend the impact of each compositional parameter on both fresh state rheology and hardened state performance.

3.3.1. Effect of activator content on printability and setting

Anhydrous sodium metasilicate powder, used as the sole solid activator in the investigated formulations, influences fresh-state rheology through several concurrent mechanisms. When mixed with water and aluminosilicate precursors, sodium metasilicate dissolves to provide hydroxyl ions and soluble silicate species, which initiate precursor dissolution and geopolymerization [37]. The activator dosage directly affects the concentration of these reactive species. This, in turn, modulates dissolution kinetics, ion mobility, and gel-formation rates and thereby influences yield stress, plastic viscosity, structural recovery, and open time.

The initial yield stress generally decreases as the activator dosage increases from 10 to 20 wt.%. Increasing the activator dosage may enhance electrostatic repulsion among precursor particles while also increasing the liquid-phase contribution to particle lubrication [38]. These effects can initially facilitate pumping and extrusion. However, the relationship is not linear. Excessive activator dosage can accelerate early-age reaction kinetics, shorten the processing window, and cause premature stiffening, which is detrimental to interlayer bonding [7]. Conversely, insufficient activator can lead to incomplete precursor dissolution [21], producing weak and highly porous gel networks that are unsuitable for structural support and layer-by-layer deposition. Among the Type-II candidate formulations, activator contents of 10%, 15%, and 20% all produced workable fresh-state behavior when appropriately balanced with GGBS proportion and aggregate loading, indicating that printability depends on interactions among mixture parameters rather than on any single parameter alone.

The structural recovery required for extrusion-based concrete printing, including shear-induced viscosity reduction during pumping and extrusion followed by rapid rebuilding after deposition, is particularly sensitive to activator chemistry and dosage [20]. Moderate activator contents can facilitate reversible breakdown and rebuilding of interparticle structures without inducing irreversible premature setting [39]. This behavior allows the material to flow under applied shear and recover sufficient yield strength after deposition, thereby supporting filament shape retention and the placement of subsequent layers.

3.3.2. Effect of GGBS Content on Printability and Setting

The setting times determined using the Vicat needle apparatus are shown in Figure. 10. The relative proportion of GGBS in the binary GGBS-fly ash precursor system influences rheological behavior and setting kinetics through both compositional and morphological effects. GGBS particles are generally more angular than the nearly spherical fly ash particles, which can increase specific surface area and interparticle friction [28]. Increasing GGBS content can therefore increase static yield stress and accelerate structural build-up, thereby improving shape retention; however, excessive GGBS may reduce extrudability and pumpability and shorten the open time [7]. The GGBS content in the six Type-II candidate mixtures was 10%, 30%, or 50%. CM-12, which exhibited the best overall printing response, contained 50% GGBS.

In addition to its particle characteristics, GGBS alters reaction chemistry because of its relatively high calcium content. Under alkaline activation, GGBS releases calcium that contributes to the formation of calcium silicate hydrate (C-S-H) and calcium aluminosilicate hydrate (C-A-S-H) gels [14]. These products generally form more rapidly than the sodium aluminosilicate hydrate (N-A-S-H) products associated predominantly with fly ash activation [14], which can promote shorter setting times and higher early-age strength. However, the present experimental results did not follow a simple GGBS-content trend. Mixtures containing 50% GGBS (CM-3, CM-12, and CM-21) exhibited initial setting times of 150-154 min, compared with 132-149 min for the 10% GGBS mixtures CM-4 and CM-7, while the corresponding final setting times were 193-207 min and 168-194 min, respectively. Thus, the measured setting behavior cannot be attributed to GGBS content alone. In particular, CM-4 and CM-7 contained higher activator dosages of 15% and 20%, respectively, which may have increased alkalinity and the availability of reactive species, thereby accelerating precursor dissolution and reaction-product formation and reducing setting time [20, 29, 30]. In these mixtures, the effect of the higher activator dosage appears to have outweighed the effect of precursor substitution. The observed setting behavior therefore reflects the combined influence of GGBS content and activator dosage rather than the intrinsic effect of GGBS alone. This interaction is important when controlling setting and structural build-up in extrusion-based 3D printing. The setting-time window, defined as the interval between initial and final setting, also affects printability and buildability. A broader window provides a longer open time but may be associated with slower structural development, whereas a narrower window can promote faster green-strength development while reducing the time available for printing.

The favorable printing performance of CM-12 resulted from the combined effects of its relatively high GGBS content and low activator dosage. The 50% GGBS content promoted structural build-up and shape retention, whereas the 10% activator dosage provided sufficient open time for continuous extrusion and interlayer bonding without causing excessive early stiffening. This balance enabled the extrusion of continuous filaments without visible discontinuities or deformation.

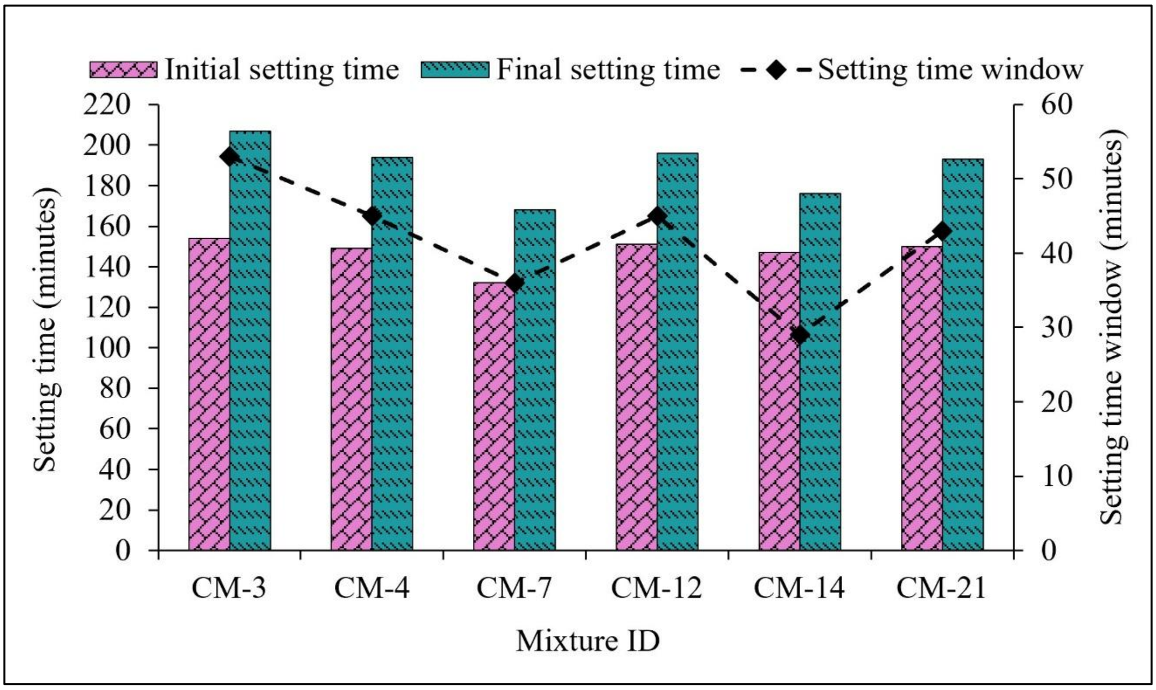

Figure 10. Setting time readings and setting time window of 3D printable mixtures in fresh state.

3.3.3. Effect on density

Material density is a measure of the effectiveness of particle packing and the properties of the gel phase [42] these factors have a major impact on the mechanical performance and longevity of the material [43]. The experimental results shown in Figure. 11 (a) and (b) indicate that the density is predictable as a function of the types of precursors, amount of aggregate and processing methods. Density of the mold-cast samples ranged from 1935 to 2217 kg/m³, while that of printed samples varied between 1792 and 2122 kg/m³.

This indicates that the layer-by-layer deposition technique consistently dropped the densities by 3.48% to 8.01 %. The density deficiency in printed specimens compared to cast specimens signifies process-induced porosity arising from multiple sources: entrapped air during extrusion, insufficient consolidation between layers, and interfacial voids at layer borders [44, 45].

Increasing GGBS content may contribute to higher hardened density through several mechanisms. First, GGBS generally has a higher specific gravity than fly ash and can influence particle packing, thereby reducing void space in GGBS-rich mixtures [46]. Second, activation of GGBS promotes the formation of calcium-bearing reaction products, including C-S-H and C-A-S-H gels, which can contribute to matrix densification relative to systems dominated by N-A-S-H products from fly ash activation [47]. In addition, accelerated reaction in high-GGBS systems may reduce capillary porosity and further increase hardened density. CM-12 achieved a mold-cast density of 2180 kg/m³, consistent with the combined effects of its precursor composition and packing characteristics.

For CM-3, CM-12, and CM-21, increasing the aggregate-to-binder ratio from 1.25 to 1.75 lowered the mold-cast density from 2217 to 2143 kg/m³; the fly-ash/GGBS proportion and activator content were held constant across this subset. This empirical trend should not be attributed solely to a presumed density difference between geopolymer paste and fine sand. Increasing aggregate content reduces paste volume and changes packing, interparticle friction, aggregate coating, and the likelihood of void formation, all of which can influence both fresh-state extrusion behavior and hardened properties [49, 51]. At the lower aggregate-to-binder ratio (1.25), greater paste availability promoted smoother flow and pumpability but could reduce shape stability under self-weight. At the higher ratio, increased aggregate contact and friction can improve dimensional stability while impairing pumpability and extrudability if the paste volume becomes insufficient [49, 51]. Accordingly, the density and strength trends observed for CM-3, CM-12, and CM-21 are interpreted as combined packing-and-paste-volume effects within the tested formulations rather than as a direct consequence of constituent density alone.

3.3.4. Effect on Compressive Strength and Mechanical Anisotropy

The compressive strength of the printed specimens was lower than that of the corresponding mold-cast specimens in the assessed directions, as shown in Figure. 12(a) and (b). The printed specimens also showed a direction-dependent response.

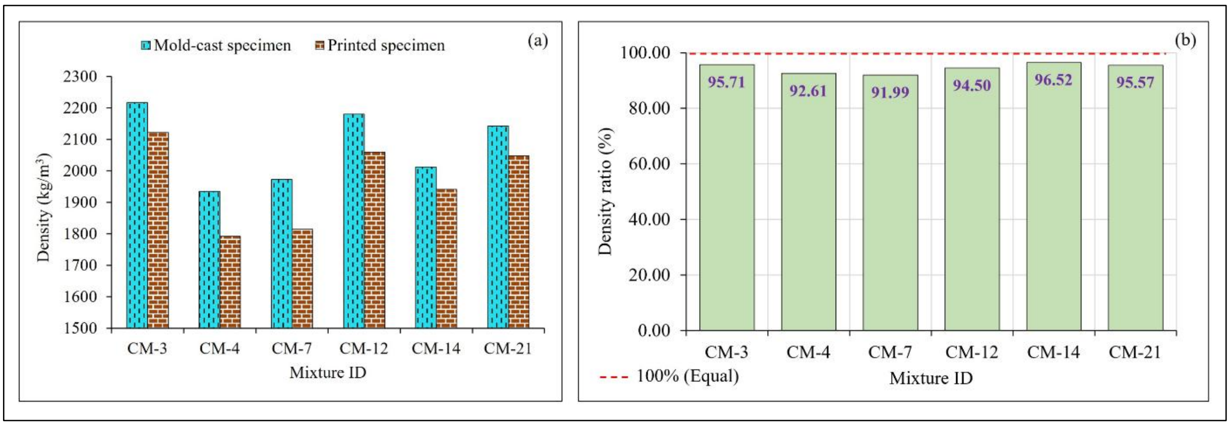

Figure 11 (a). Average density of mold-cast and printed specimens for the printable mixtures and **(b)** printed to mold-cast density ratio (%) for the printable mixtures

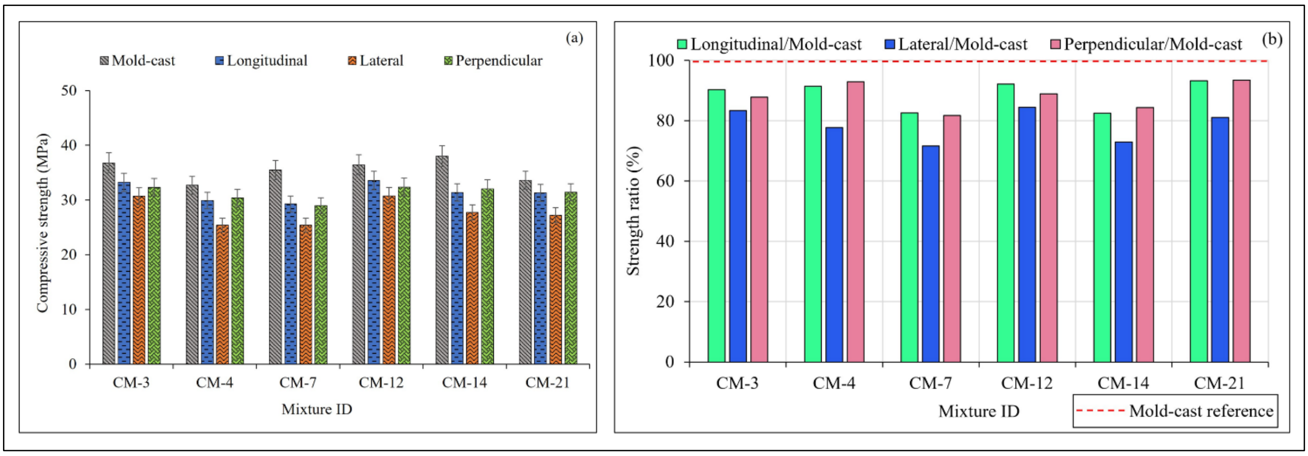

Figure 12 (a). Compressive strength in different tested directions of mold-cast and printed samples for the formulated mixtures and **(b)** printed-to-mold-cast compressive-strength ratio (%) for the printable mixtures. Values in (a) are means of three specimens; the plotted error bars show replicate variability. No inferential significance across orientations is claimed.

The lateral direction was the lowest-strength orientation for all six printable mixtures, whereas the longitudinal and perpendicular values were closer to one another and the higher of these two directions varied among mixtures. Similar direction-dependent behavior has been reported for extrusion-printed cementitious and geopolymer materials [28, 50]. Each plotted strength value represents the mean of three specimens. Because the available replicate set was not analyzed with an orientation-specific inferential test, the results are described as observed directional differences rather than as statistically significant anisotropy. The 28-day mold-cast compressive strengths ranged from 32.7 to 41.29 MPa, confirming that the screened formulations developed structural-level matrix strength within the conditions of this study.

Higher GGBS proportion produces additional C–S–H and denser microstructure, enhancing compressive strength; activator dose must be sufficient to dissolve precursors and form gels but low enough to preserve interlayer bonding time during printing [46, 47]. Strength of the composite was influenced by activator content via its effect on extent of reaction and gelation. Intermediate activator dosages (10–15%) were high enough to achieve the necessary alkalinity for relatively fast precursor solubilization but low enough not to produce high hydroxyl concentrations that would interfere with gel polymerization or cause crystallization [39, 47]. The extent of strength reduction of printed specimens in comparison to their mold-cast counterparts is contingent upon composition, printing time intervals, rheology, and curing conditions. Mixtures with elevated activator content (CM-4, CM-7, CM-14) showed larger strength decreases likely attributable to accelerated setting that constrained interlayer adhesion. Conversely, combinations containing 10% activator (CM-3, CM-12, CM-21) exhibited diminished strength reductions indicating that a slower setting facilitates enhanced interlayer adhesion.

CM-12 showed comparatively balanced longitudinal and perpendicular strength retention together with the lowest lateral strength, while maintaining good printing performance. Its composition—50% GGBS, an aggregate-to-binder ratio of 1.5, and 10% activator—provided a practical balance between precursor reactivity, paste availability, open time, and shape retention. The present data therefore suggest that composition can influence the magnitude of directional strength differences, but they do not establish a statistically significant reduction in anisotropy. Further work using replicate-level orientation statistics and direct interlayer-bond measurements is required to quantify this effect.

3.3.5. Integrated mix design optimization

Overall, CM-12 provided the most favorable balance among printability, density, setting behavior, and mechanical performance. Its 50% GGBS content provided a calcium-rich precursor fraction that supported reaction-product formation, structural build-up, and strength development, while the remaining fly ash helped maintain workability. The aggregate-to-binder ratio of 1.5 balanced the paste volume required for pumpability with the aggregate skeleton needed for dimensional stability. The 10% activator dosage provided sufficient activation while limiting premature stiffening and maintaining an adequate processing window. These parameters interact rather than act independently; the benefits of 50% GGBS for strength and buildability depend on sufficient paste volume and controlled activator dosage.

This integrated optimization approach proves essential for advancing 3D-printable geopolymer concrete from laboratory demonstration to practical construction applications, where materials must satisfy stringent performance requirements across fresh-state processing, early-age structural development, and long-term mechanical durability.

4. Conclusions

This study investigated the combined effects of precursor composition, activator dosage, and aggregate loading on the fresh-state behavior, printability, and mechanical performance of one-part geopolymer concrete. The principal technical conclusions are summarized below.

- Potential field-oriented consistency assessment: The developed "bucket test" provided a rapid qualitative screening of fresh mix consistency. Its Type I–IV classifications showed good agreement with flow-table behavior, but printing trials of the six Type-II candidates showed that only CM-12 and CM-21 met the strict combined criterion of delivery, continuous extrusion, and acceptable filament stability. The method should therefore be used as a low-cost preliminary screening tool together with quantitative flow tests and printing verification, not as a stand-alone predictor of printability.
- Printable region determination: For the investigated materials and printer configuration, the candidate printability region was associated with zero slump and a slump-flow diameter of 140-180 mm. A further practical indicator was the reduction in slump flow after a 10 min rest period, which was typically 10-15 mm for the Type-II candidate mixtures and represented a balance between pumpability and structural build-up.
- Optimal mix design: CM-12, containing 50% GGBS, 50% fly ash, an aggregate-to-binder ratio of 1.5, and 10% activator, exhibited the best overall printing response. This combination provided sufficient structural recovery for shape retention while maintaining an adequate open time, enabling continuous printing of a 12-layer object without visible distortion or interfacial gaps.
- Hardened state properties and directional response: The 3D-printed specimens showed a density reduction of 3.48% to 8.01% relative to mold-cast specimens. Compressive strength was direction-dependent, with the lateral direction consistently giving the lowest values while longitudinal and perpendicular strengths were generally higher. Because only three specimens were tested per orientation and no orientation-specific inferential test was performed, these differences are reported descriptively rather than as statistically significant anisotropy. The mold-cast mixtures developed 28-day compressive strengths of 32.7 to 41.29 MPa.

4.1. Importance and Relevance

This study provides a practical contribution toward improving the logistical feasibility of one-part geopolymer construction. The one-part binder avoids handling of caustic liquid activators, while the proposed bucket test offers a simple preliminary consistency screen that can be performed with limited equipment. However, the method is not a replacement for rheometry or direct printing verification, and its numerical screening limits are specific to the materials and equipment used in this study.

4.2. Limitations and Scope of Applicability

The proposed bucket-test methodology and the identified printability window should be interpreted within the experimental conditions of the present study. The reported limits were established using the investigated GGBS–fly ash one-part geopolymer formulations, a controlled temperature of 27 ± 2 °C, the selected fine-sand grading, a 30 mm nozzle, a 50 mm delivery hose, and the specific three-axis gantry-type printing system.

Only the six Type-II candidate mixtures were subjected to extrusion trials; therefore, sensitivity, specificity, and false-negative rates of the bucket classification cannot be determined from this dataset. Moreover, the bucket assessment retains operator-dependent qualitative observations such as adhesion, tactile roughness, and furrow closure. The printing campaign recorded average filament width, but post-deposition filament height and dimensional variation along the full 1000 mm filament were not systematically measured. Variations in ambient temperature, material moisture, aggregate grading, mixing procedure, hose length, nozzle geometry, pumping pressure, printing speed, and equipment configuration may alter fresh-state and extrusion behavior. Accordingly, the 140–180 mm slump-flow range and 10–15 mm 10-min flow-loss criterion should be treated as material- and equipment-specific screening values, not as universal field quality-control limits. Further validation across independent material sources, operators, environmental conditions, and printer configurations is required before standardized site-control thresholds can be proposed.

4.3. Future Scope

Microstructure characterization: SEM, XRD, MIP measurements should be included in further studies to relate the evolution of the gel and its pore structure to the mechanical anisotropy observed.

Long-term durability: Research is necessary for evaluating the long-term durability, i.e., shrinkage, creep, carbonation resistance, and chloride permeability of printed one-part geopolymer concrete members.

Structural application: It is important for structural applications to verify the compatibility of this optimized mix with automatic reinforcement methods (e.g., addition of micro-fiber or winding a cable).

Environmental life-cycle assessment: Future work should compare the life-cycle carbon footprint of the proposed one-part geopolymer mixture with that of conventional 3D-printable Portland-cement mixtures to quantify its potential environmental benefits.

References

[1] G. Anand, T.N. Tharunkumar, Review on partial replacement of cement in concrete by using waste materials. International Research Journal of Multidisciplinary Technovation, 1(6), (2019) 526-531. https://doi.org/10.34256/irjmtcon76

[2] H. Zhong, M. Zhang, 3D printing geopolymers: A review. Cement and Concrete Composites, 128, (2022) 104455. https://doi.org/10.1016/j.cemconcomp.2022.104455

[3] R. Ranjith, P. Easwaran, M. Kalaivani, S. Ramesh, Strength and Structural Properties of Geopolymer Concrete with Natural Fibers—A Review. International Research Journal of Multidisciplinary Technovation, 1, (2019) 432–438. https://doi.org/10.34256/irjmtcon60

[4] A. Vinothkumar, M. Kalaivani, P. Easwaran, Development of fly ash GGBS based self compacting geopolymer concrete: A review. International Research Journal of Multidisciplinary Technovation, 1(6), (2019) 373–377. https://doi.org/10.34256/irjmtcon49

[5] C. Roux, J. Archez, C. Le Gall, M. Saadé, A. Féraille, J.-F. Caron, Towards sustainable material: optimizing geopolymer mortar formulations for 3D printing: a life cycle assessment approach. Sustainability, 16(8), (2024) 3328. https://doi.org/10.3390/su16083328

[6] B. Panda, S.C. Paul, L.J. Hui, Y.W.D. Tay, M.J. Tan, Additive manufacturing of geopolymer for sustainable built environment. Journal of Cleaner Production, 167, (2017) 281–288. http://dx.doi.org/10.1016/j.jclepro.2017.08.165

[7] S.H. Bong, M. Xia, B. Nematollahi, C. Shi, Ambient temperature cured 'just-add-water' geopolymer for 3D concrete printing applications. Cement and Concrete Composites, 121, (2021) 104060. https://doi.org/10.1016/j.cemconcomp.2021.104060

[8] K. Avinash Varma, K.S. Chundury, B. Narendra Kumar, A Review on Application of 3D Printing Principles in Infrastructure Industry and its Impact on Evolution of the Industry. International Research Journal of Multidisciplinary Technovation, 4(4), (2022) 1–7. https://doi.org/10.54392/irjmt2241

[9] M. Priyadharshini, S.S. Chelladurai, Best Mix Ratio for Concrete Printing using Localised Materials. International Research Journal of Multidisciplinary Technovation, 2(3), (2020) 22–26. https://doi.org/10.34256/irjmt2034

[10] T.D. Ngo, A. Kashani, G. Imbalzano, K.T. Nguyen, D. Hui, Additive manufacturing (3D printing): A review of materials, methods, applications and challenges. Composites Part B: Engineering, 143, (2018) 172–196. https://doi.org/10.1016/j.compositesb.2018.02.012

[11] P. Barve, A. Bahrami, S. Shah, A Comprehensive Review on Effects of Material Composition, Mix Design, and Mixing Regimes on Rheology of 3D-Printed Geopolymer Concrete. The Open Construction & Building Technology Journal, 18, (2024). https://doi.org/10.2174/0118748368292859240313061706

[12] D. Sharma, R.B. Singh, A. Gupta, A State-Of-The-Art Review on Development and Properties of One-Part Geopolymer Materials. Advances in

Civil Engineering, 2025(1), (2025) 8856426. https://doi.org/10.1155/adce/8856426

[13] B. Panda, C. Unluer, M.J. Tan, Investigation of the rheology and strength of geopolymer mixtures for extrusion-based 3D printing. Cement and Concrete Composites, 94, (2018) 307–314. https://doi.org/10.1016/j.cemconcomp.2018.10.002

[14] D. Sun, J. Lee, A. Mohyeddin, J. Migunthanna, Mechanical Properties and Reproducibility of One-Part Ambient-Cured Slag and Fly Ash-Based Geopolymer Concrete. Buildings, 16(4), (2026) 707. https://doi.org/10.3390/buildings16040707

[15] J. Ren, H. Sun, Q. Li, Z. Li, L. Ling, X. Zhang, Y. Wang, F. Xing, Experimental comparisons between one-part and normal (two-part) alkali-activated slag binders. Construction and Building Materials, 309, (2021) 125177. https://doi.org/10.1016/j.conbuildmat.2021.125177

[16] B. Nematollahi, J. Sanjayan, F.U.A. Shaikh, Synthesis of heat and ambient cured one-part geopolymer mixes with different grades of sodium silicate. Ceramics International, 41(4), (2015) 5696–5704. https://doi.org/10.1016/j.ceramint.2014.12.154

[17] A. Kul, O. Kocaer, A. Aldemir, G. Yildirim, S.S. Lucas, 3D printable one-part alkali-activated mortar derived from brick masonry wastes. Case Studies in Construction Materials, 21, (2024) e04081. https://doi.org/10.1016/j.cscm.2024.e04081

[18] G. Ma, Y. Yan, M. Zhang, J. Sanjayan, Effect of steel slag on 3D concrete printing of geopolymer with quaternary binders. Ceramics International, 48(18), (2022) 26233–26247. https://doi.org/10.1016/j.ceramint.2022.05.305

[19] Y.A. Al-Noaimat, S.H. Ghaffar, M. Chougan, M.J. Al-Kheetan, A review of 3D printing low-carbon concrete with one-part geopolymer: Engineering, environmental and economic feasibility. Case Studies in Construction Materials, 18, (2023) e01818. https://doi.org/10.1016/j.cscm.2022.e01818

[20] S. Muthukrishnan, S. Ramakrishnan, J. Sanjayan, Effect of alkali reactions on the rheology of one-part 3D printable geopolymer concrete. Cement and Concrete Composites, 116, (2021) 103899. https://doi.org/10.1016/j.cemconcomp.2020.103899

[21] B. Panda, G.B. Singh, C. Unluer, M.J. Tan, Synthesis and characterization of one-part geopolymers for extrusion-based 3D concrete printing. Journal of Cleaner Production, 220, (2019) 610–619. https://doi.org/10.1016/j.jclepro.2019.02.185

[22] B. Nematollahi, S.H. Bong, M. Xia, J. Sanjayan, Digital Fabrication of 'Just-Add-Water' Geopolymers: Effects of Curing Condition and Print-Time Interval. In: Bos, F., Lucas, S., Wolfs, R., Salet, T. (eds) Second RILEM International Conference on Concrete and Digital Fabrication. DC 2020. RILEM Bookseries, Springer, Cham, 28, (2020) 93–102. https://doi.org/10.1007/978-3-030-49916-7_10

[23] B. Nematollahi, M. Xia, S.H. Bong, J. Sanjayan, Hardened Properties of 3D Printable 'One-Part' Geopolymer for Construction Applications. In: Wangler, T., Flatt, R. (eds) First RILEM International Conference on Concrete and Digital Fabrication – Digital Concrete 2018. DC 2018. RILEM Bookseries, Springer, Cham, 19, (2018) 190–199. https://doi.org/10.1007/978-3-319-99519-9_17

[24] Y. Zhang, Y. Zhang, G. Liu, Y. Yang, M. Wu, B. Pang, Fresh properties of a novel 3D printing concrete ink. Construction and Building Materials, 174, (2018) 263–271. https://doi.org/10.1016/j.conbuildmat.2018.04.115

[25] O.H. Wallevik, D. Feys, J.E. Wallevik, K.H. Khayat, Avoiding inaccurate interpretations of rheological measurements for cement-based materials. Cement and Concrete Research, 78, (2015) 100–109. https://doi.org/10.1016/j.cemconres.2015.05.003

[26] S.C. Figueiredo, C.R. Rodríguez, Z.Y. Ahmed, D.H. Bos, Y. Xu, T.M. Salet, O. Çopuroğlu, E. Schlangen, F.P. Bos, An approach to develop printable strain hardening cementitious composites. Materials & Design, 169, (2019) 107651. https://doi.org/10.1016/j.matdes.2019.107651

[27] S.H. Bong, B. Nematollahi, A. Nazari, M. Xia, J. Sanjayan, Efficiency of different superplasticizers and retarders on properties of 'One-Part' Fly ash-slag blended geopolymers with different activators. Materials, 12(20), (2019) 3410. https://doi.org/10.3390/ma12203410

[28] K. Pasupathy, S. Ramakrishnan, J. Sanjayan, 3D concrete printing of eco-friendly geopolymer containing brick waste. Cement and Concrete Composites, 138, (2023) 104943. https://doi.org/10.1016/j.cemconcomp.2023.104943

[29] J. Hou, X. Zhang, C. Zhang, J. Wang, P. Zheng, J. Huang, S. Feng, J. Wang, G. Duan, Adjusting the early rheology of alkali-activated slag by sodium silicate. Case Studies in Construction Materials, 21, (2024) e03995. https://doi.org/10.1016/j.cscm.2024.e03995

[30] Y. Sun, M.K. Mohan, X. Dai, Y. Zhang, G. Ye, G. De Schutter, Effects of mixing conditions and activator anionic species on the rheology of silicate-activated slag concrete. Cement and

Concrete Composites, 150, (2024) 105556. https://doi.org/10.1016/j.cemconcomp.2024.105556

[31] P. Sahoo, S. Gupta, 3D printable earth-based alkali activated "ink": effect of alkali concentration and binder-to-aggregate ratio. Journal of Building Engineering, 98, (2024) 111208. https://doi.org/10.1016/j.jobe.2024.111208

[32] J. Davidovits, (2008). Geopolymer chemistry and applications, 5th ed. Geopolymer Institute. https://www.geopolymer.org/learning/book-geopolymer-chemistry-and-applications/

[33] P. Barve, A. Bahrami, S. Shah, Geopolymer 3D printing: a comprehensive review on rheological and structural performance assessment, printing process parameters, and microstructure. Frontiers in Materials, 10, (2023) 1241869. https://doi.org/10.3389/fmats.2023.1241869

[34] S. Hou, Z. Duan, J. Xiao, J. Ye, A review of 3D printed concrete: Performance requirements, testing measurements and mix design. Construction and Building Materials, 273, (2021) 121745. https://doi.org/10.1016/j.conbuildmat.2020.121745

[35] Y.A. Al-Noaimat, M. Chougan, A. Albar, S. Skibicki, K. Federowicz, M. Hoffman, D. Sibera, K. Cendrowski, M. Techman, J.N. Pacheco, S.Y. Chung, P. Sikora, M. Al-Kheetan, S.H. Ghaffar, Recycled brick aggregates in one-part alkali-activated materials: Impact on 3D printing performance and material properties. Developments in the Built Environment, 16, (2023) 100248. https://doi.org/10.1016/j.dibe.2023.100248

[36] Y.W.D. Tay, Y. Qian, M.J. Tan, Printability region for 3D concrete printing using slump and slump flow test. Composites Part B: Engineering, 174, (2019) 106968. https://doi.org/10.1016/j.compositesb.2019.106968

[37] E. Kamseu, V. Alzari, D. Nuvoli, D. Sanna, I. Lancellotti, A. Mariani, C. Leonelli, Dependence of the geopolymerization process and end-products to the nature of solid precursors: Challenge of the sustainability. Journal of Cleaner Production, 278, (2021) 123587. https://doi.org/10.1016/j.jclepro.2020.123587

[38] J. Yang, G. Zhai, X. He, Y. Tang, Y. Su, X. Yu, J. Zeng, F. Wang, Properties and microstructure of a low-carbon clinker-free cementitious binder and its extrusion-based printing performance. Journal of Building Engineering, 90, (2024) 109483. https://doi.org/10.1016/j.jobe.2024.109483

[39] Q. Yuan, C. Gao, T. Huang, S. Zuo, H. Yao, K. Zhang, Y. Huang, J. Liu, Factors influencing the properties of extrusion-based 3D-printed alkali-activated fly ash-slag mortar. Materials, 15(5), (2022) 1969. https://doi.org/10.3390/ma15051969

[40] F.A. Shilar, S.V. Ganachari, V.B. Patil, T.Y. Khan, S. Javed, R.U. Baig, Optimization of alkaline activator on the strength properties of geopolymer concrete. Polymers, 14(12), (2022) 2434. https://doi.org/10.3390/polym14122434

[41] O.A. Mohamed, R. Al Khattab, W. Al Hawat, Effect of relative GGBS/fly contents and alkaline solution concentration on compressive strength development of geopolymer mortars subjected to sulfuric acid. Scientific Reports, 12(1), (2022) 5634. https://doi.org/10.1038/s41598-022-09682-z

[42] M. Samudrala, S. Mujeeb, B.A. Lanjewar, R. Chippagiri, M. Kamath, R.V. Ralegaonkar, 3D-Printable Concrete for Energy-Efficient Buildings. Energies, 16(10), (2023) 4234. https://doi.org/10.3390/en16104234

[43] L. Zhu, M. Zhang, Y. Zhang, J. Yao, G. Yang, X. Guan, Y. Zhao, Research progress on shrinkage properties of extruded 3D printed cement-based materials. Journal of Building Engineering, 77, (2023) 107394. https://doi.org/10.1016/j.jobe.2023.107394

[44] P. Sikora, M. Techman, K. Federowicz, A.M. El-Khayatt, H.A. Saudi, M. Abd Elrahman, M. Hoffmann, D. Stephan, S.-Y. Chung, Insight into the microstructural and durability characteristics of 3D printed concrete: Cast versus printed specimens. Case Studies in Construction Materials, 17, (2022) e01320. https://doi.org/10.1016/j.cscm.2022.e01320

[45] A. Das, Y. Song, S. Mantellato, T. Wangler, D.A. Lange, R.J. Flatt, Effect of processing on the air void system of 3D printed concrete. Cement and concrete research, 156, (2022) 106789. https://doi.org/10.1016/j.cemconres.2022.106789

[46] Z. Zhou, J. Geng, C. Jin, G. Liu, Z. Xia, Influence of Residue Soil on the Properties of Fly Ash–Slag-Based Geopolymer Materials for 3D Printing. Materials, 17(12), (2024) 2992. https://doi.org/10.3390/ma17122992

[47] M. Elzeadani, D.V. Bompa, A.Y. Elghazouli, One part alkali activated materials: A state-of-the-art review. Journal of Building Engineering, 57, (2022) 104871. https://doi.org/10.1016/j.jobe.2022.104871

[48] G. Gaurav, S.C. Kandpal, D. Mishra, N. Kotoky, A comprehensive review on fly ash-based geopolymer: a pathway for sustainable future. Journal of Sustainable Cement-Based Materials, 13(1), (2024) 100–144. https://doi.org/10.1080/21650373.2023.2258122

[49] M. Gurunandan, H.J. Malla, P. Nanthagopalan, Effect of water to binder, aggregate to binder ratio and admixtures on printability and mechanical

properties of 3D printable mortar mixtures. Journal of Building Engineering, 99, (2025) 111649. https://doi.org/10.1016/j.jobe.2024.111649

[50] S.C. Paul, Y.W.D. Tay, B. Panda, M.J. Tan, Fresh and hardened properties of 3D printable cementitious materials for building and construction. Archives of Civil and Mechanical Engineering, 18(1), (2018) 311–319. https://doi.org/10.1016/j.acme.2017.02.008

[51] J.-C. Xue, W.-C. Wang, M.-G. Lee, C.-Y. Huang, C.-Y. Liang, Effect of aggregate-to-binder ratio on 3D printed concrete: printability, mechanics, and shrinkage. Materials and Structures, 59(1), (2026) 14. https://doi.org/10.1617/s11527-025-02866-9

Acknowledgment

Authors acknowledge the support from the Cretebots Digital Constructions Private Limited, Pune, Maharashtra, India for 3D printing facility.

Authors Contribution Statement

Prasad Barve: Writing – Original Draft, Visualization, Validation, Methodology, Resources, Investigation, Formal analysis, Data curation, Conceptualization. Deep Upadhyaya: Writing – Review & Editing, Project Administration, Supervision. Santosh Shah: Writing – Review & Editing, Visualization, Validation, Supervision, Project administration, Conceptualization. All the authors have read and agreed to the published version of the manuscript.

Funding

The authors declare that no funds, grants or any other support were received during the preparation of this manuscript.

Competing Interests

The authors declare that there are no conflicts of interest regarding the publication of this manuscript.

Data Availability

The data supporting the findings of this study can be obtained from the corresponding author upon reasonable request.

Has this article screened for similarity?

Yes

About the License